Research Article | Vol. 26, No. 26 | 24 Dec 2018 | OPTICS EXPRESS 34965
Optics EXPRESS

Direct thermo-optical tuning of silicon microresonators for the mid-infrared

L. Koehler,[1,2,5] P. Chevalier,[1,5] E. Shim,[3] B. Desiatov,[1], A. Shams-Ansari,[1] M. Piccardo,[1] Y. Okawachi,[4] M. Yu,[4] M. Loncar,[1] M. Lipson,[3] A. L. Gaeta,[4] and F. Capasso[1,*]

[1]Harvard John A. Paulson School of Engineering and Applied Science, Cambridge, MA 02138, USA
[2]Ecole Polytechnique, 91123 Palaiseau, France
[3]Department of Electrical Engineering, Columbia University, New York, New York 10027, USA
[4]Department of Applied Physics and Applied Mathematics, Columbia University, New York, NY 10027, USA
[5]These authors contributed equally to this work.
[*]capasso@seas.harvard.edu

Abstract: We use light from a visible laser diode to directly tune silicon-on-chip microresonators by thermo-optical effect. We show that this direct tuning is local, non invasive and has a much smaller time constant than global temperature tuning methods. Such an approach could prove to be highly effective for Kerr comb generation in microresonators pumped by quantum cascade lasers, which cannot be easily tuned to achieve comb generation and soliton-modelocked states.

1. Introduction

Microresonators are a reliable way to generate frequency combs by four-wave mixing (FWM) via the Kerr non-linearity of their medium [1] and in the near-infrared, an octave spanning frequency comb was demonstrated using a silicon nitride microresonator [2]. Thanks to its low linear and two-photon absorption in the mid-IR, its high Kerr non-linearity and its well established processing, silicon is a material of choice for the generation of frequency combs in the mid-IR using integrated high quality-factor ring resonators. Recently, integrated resonators have been used with a pump wavelength as long as 3.8 μm to generate frequency combs [3]. Quantum cascade lasers (QCLs) can be used as standalone sources for frequency comb generation [4, 5]. However, the total width of their comb state is ultimately limited by the bandwidth of the gain medium. QCLs can be tuned to emit watt-level single-mode radiation [6] and have also been successfully integrated with silicon-based photonics [7]. Therefore, one may envision a fully integrated platform for frequency comb generation combining QCLs and silicon ring resonators. To obtain frequency comb generation with Kerr resonators, the emission frequency of the pump laser has to be properly tuned into a ring resonance [8]. When working with crystalline resonators this tuning can be achieved mechanically by using a piezo-electric transducer [9]. For a resonator integrated on a chip a conventional way to tune the ring resonance into the pump frequency is by using a thermo-electric cooler (TEC). However, this method suffers from a long time-constant [10]. Thermal tuning can be achieved with a much shorter time constant by integrating micro-heaters near the resonators [11, 12] providing the proper tuning speed to generate frequency combs. Alternatively, the integration of a PiN diode with the microresonator can be used to control the free carrier concentration as a reliable and fast way to generate frequency combs [3]. Finally, thermo-optical tuning has also been studied by using a tuning beam that shares the same waveguide as the pump beam and is used to thermally tune the resonator through light absorption [13].

Here we present a different approach for direct thermo-optical tuning of silicon resonators operating in the mid-IR that consists of focusing light from a laser diode emitting around 450 nm directly on the ring resonator. This method is applied to two different platforms for integrated

#349343 https://doi.org/10.1364/OE.26.034965
Journal © 2018 Received 29 Oct 2018; revised 8 Dec 2018; accepted 11 Dec 2018; published 21 Dec 2018

Optics EXPRESS

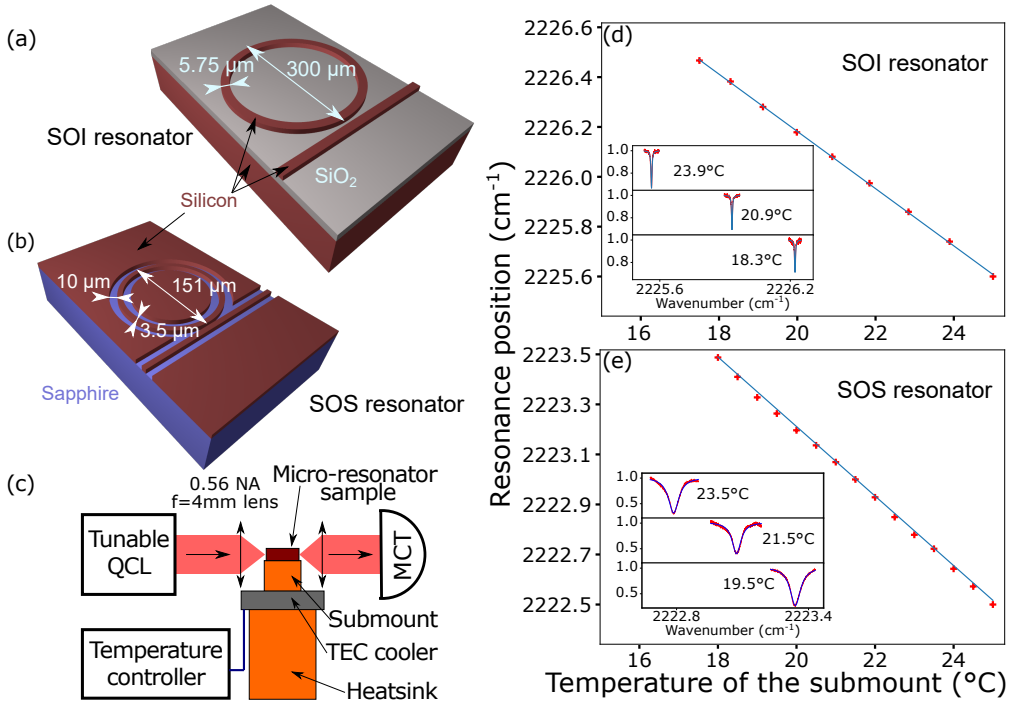

Fig. 1. (a) Schematic of a silicon on insulator (SOI) resonator device showing the waveguide and the ring resonator. The SiO_2 layer is 4 micron thick, the top and bottom silicon layers are respectively 3.3 µm and 500 µm thick. (b) Schematic of the silicon on sapphire (SOS) resonator device showing the waveguide, the ring resonator and the unetched neighboring silicon. The sapphire layer is 650 µm thick and the silicon is 1 µm thick. (c) The transmission of the waveguide coupled to the resonator under study is measured as function of the quantum cascade laser (QCL) frequency with a HgCdTe (MCT) detector. The temperature of the submount is stabilized and tuned to different set-points using a thermo-electric cooler (TEC) and a temperature controller. while tuning the temperature of the submount. Plot of the position of the ring resonance in wavenumber units as a function of the submount temperature: (d) for the SOI resonators and (e) for the SOS resonators. Inset: the transmitted QCL signal is plotted as a function of the wavenumber at three different temperatures, showing the shift of the resonance.

photonics in the Mid-IR : Silicon on sapphire (SOS) resonators [14] and Silicon on insulator (SOI) resonators [15]. The absolute shift of the resonance frequency is first measured while tuning the temperature with a TEC as a reference point. The direct thermo-optical method is then introduced and the resonance shift measured as a function of the laser diode power. Numerical simulations compared to measurements of the resonance shift as function of the laser position show the locality of the thermo-optical tuning. Finally we report the time constant of such a tuning method by modulating the laser power at various frequencies.

2. Silicon microresonators and thermo-electric tuning

In the following, the tuning properties of two different integrated resonators are studied. The first consists of a ring resonator made from an SOI wafer [15]. The silicon ring resonator is 3.3 µm thick and 5.75 µm wide with a ring diameter of 300 µm and 4 µm thick buried oxide (BOX) layer. The silicon substrate is 500 µm (see Fig. 1(a)). The chip is fabricated by means of electron beam lithography and dry etching of a commercial SOI wafer [15]. The free-spectral range (FSR) of

Optics EXPRESS

this resonator has been estimated by simulation: $\mathrm{FSR_{SOI}} = 3\,\mathrm{cm}^{-1}$. The second device is a silicon on sapphire (SOS) resonator. A 1 µm thick silicon film is bonded to a 650 µm thick sapphire substrate. The silicon film is then patterned by electron beam lithography followed by etching into a ring (width: 3.5 µm, diameter 150 µm). The free-spectral range of this resonator has been estimated by simulation: $\mathrm{FSR_{SOS}} = 6\,\mathrm{cm}^{-1}$. Due to the difference in fabrication compared to the other platforms, some unetched silicon remains on the chip around the resonator at a minimum distance of 10 µm as outlined on Fig. 1(b).

A schematic of the experimental setup used to study the position of the resonance frequency of the microresonators is shown in Fig. 1(c). The microresonator is mounted on a thermo-electrically cooled (TEC) stage (cooling element: Custom thermoelectrics 05001-9G30-35RU7F) with a temperature feedback provided by a 10 $k\Omega$ thermistor. A closed-loop temperature controller (Wavelength electronic TC5) maintains the temperature of the submount constant within 10 mK of a given setpoint. Light from a mid-IR External-cavity quantum cascade laser (EC-QCL, Daylight Solutions 21043MHF) is coupled into the waveguide using an aspheric lens (Thorlabs C036TME, f=4mm, NA 0.56). The light from the waveguide is collected using a similar aspheric lens and sent into a TEC-cooled HgCdTe (MCT) detector (Vigo PVI-4TE-10.6). The QCL emission wavenumber can be continuously tuned over a $1.2\,\mathrm{cm}^{-1}$ range around a variable center frequency by using the integrated piezo-electric transducer of the EC-QCL. This tuning method allows the acquisition of the device transmission as a function of the wavenumber. As the QCL is tuned into a resonance of the ring, light is extinguished and a minimum of the transmission is observed at resonance. This tuning method was calibrated by sending the light from the QCL into a Michelson interferometer of known path difference. When measuring the transmission of the resonator by this technique, the laser power is strongly attenuated to avoid thermal broadening of the resonance [16] and we estimate that the power of the mid-IR light coupled into the waveguide is approximately 10 µW.

To characterize the influence of the temperature on the ring resonator, the resonance position is measured for variable temperatures of the submount between 18°C and 25°C. The measured resonance position for SOI resonators (resp. SOS resonators) is plotted in Fig. 1(d) (resp. Fig. 1(e)) as a function of the temperature of the submount. This figure shows that for both of these resonators as the submount temperature increases, the resonance frequency decreases. The tuning rate of this method, defined as the slope of the linear fit of the resonance position as function of the temperature, is $-3.4\,\mathrm{GHz/K}$ for the SOI and $-4.2\,\mathrm{GHz/K}$ for the SOS resonator. Normalized by the respective free spectral range of each resonator, the thermal tuning speed is $-3.8 \times 10^{-2}\,\mathrm{FSR/K}$ for the SOI and $-2.3 \times 10^{-2}\,\mathrm{FSR/K}$ for the SOS resonator.

This behavior is explained as follows: increasing the temperature of the resonator increases the refractive index of silicon and thus increase the effective index n of the whispering gallery mode in the resonator. As a consequence, the frequency of the p-th mode of the resonator $\nu_p = pc/(2\pi Rn)$, where R is the resonator radius, is shifted towards lower frequencies.

A lorentzian fit of the resonance enables the deduction of the width of each resonance, for a given temperature. As shown in insets of Figs. 1(d) and 1(e), the temperature variation only changes the position of the resonances. Their relative extinctions and quality factors remain unchanged. These plots also show the difference in quality factor of these two resonators: 10^6 and 10^5 for the SOI and SOS resonator, respectively.

3. Thermo-optical tuning

In this section we study how the local heating from a visible laser diode can be used to tune the resonance of silicon resonators. The light from a laser diode emitting around 450 nm (Osram PL-450B) is collimated with an aspheric anti-reflection (AR) coated lens (Thorlabs C330TMD, $f = 3.1$ mm , NA 0.68), and finally focused on the resonator device with a bi-convex AR coated lens (Thorlabs LB1471, $f = 50$ mm, $d = 25$ mm). At this wavelength the absorption coefficient

Optics EXPRESS

of silicon [17] $\alpha_{Si}(450\,nm) = 26000\,cm^{-1}$ is more than ten times larger than at 650 nm, which justifies the use of this particular wavelength in the following study. This optical system is mounted on a 3-axis motorized stage, allowing the independent control of the spot position on the sample (x- and y-axis) and the focus of the spot (z-axis). The schematic of this setup is shown in Fig. 2(a). The spot size produced by this optical system has been calibrated as a function of the z position by illuminating a CMOS camera whose sensor was placed at the same height as the resonator and by processing the resulting image. Due to the anisotropic divergence of the laser diode the spot was elliptical. In the focal plane a beam waist of 40 μm was measured along the x-axis, and a waist of 13 μm was measured in the orthogonal direction. For a two-dimensional scan of the x and y-axis stage over 300 μm, the positioning error of the laser spot was determined to be below 7 μm. In order to to study the response of the resonator illuminated up with a larger beam, we determined a position of the z-axis stage resulting in a spot of dimensions $w_x = 106$ μm, $w_y = 49$ μm on the resonator. With such an optical setup, light from the blue laser can be used to induce a local heating of the device and thus tune the resonator accordingly.

3.1. Direct tuning by varying the laser power

The influence of the optical power of the tuning laser on the shift of the resonance is first studied for both resonators. The laser diode was operated at room temperature and driven by a constant current generator (Keithley 2400 Sourcemeter) between 0 mA and 80 mA. Lasing was obtained for a threshold of 20 mA, and over this current range the optical power focused by the optical system was between 0 and 60 mW. Those measurements were taken after optimizing the position of the laser spot on the chip to obtain the largest resonance shift. The optimal position for the laser spot was found to be on or close to the edge of the ring resonator. As shown in Figs. 2(b) and 2(c), the measured resonance position evolves linearly with the optical power of the tuning laser, and is shifted up to $0.4\,cm^{-1}$ within this range of optical power. In this case, the tuning rate of the resonator per the optical power of the tuning laser is estimated as -191 MHz/mW for the SOI resonator and -194 MHz/mW for the SOS resonator. Normalized by the respective free spectral range of each resonator, the optical tuning speed is -2.13×10^{-3} FSR/mW for the SOI and -1.09×10^{-3} FSR/mW for the SOS resonator.

The bottom-left insets show the QCL transmitted signal as a function of the tuning frequency. As opposed to the measurement performed with TEC tuning, the resonance Q-factor is also reduced as the optical power increases, especially for the SOI resonator. The dependence of the Q-factor as a function of the laser power is plotted in the top-right insets of Figs. 2 (b) and 2(c). The decrease of the Q-factor can be explained by the creation of free-carriers in silicon that enhance the ring losses in the mid-IR. Increasing the losses of the ring resonator can be detrimental for Kerr comb generation as a decrease in the Q-factor will quadratically raise the threshold for four-wave mixing. However, here the Q-factor remains within 90% of its initial value when the power of the heating laser is maintained below 15 mW. For comb generation, we envision to combine this technique with a coarser TEC tuning and only use the lowest possible power on the tuning laser.

3.2. Modeling of the thermo-optical tuning

Thermal modeling enables to predict the experimental results since the temperature values computed within the material can be related to the measured resonance shift values obtained by TEC tuning (see Fig. 1). Equation (1) is the stationary heat equation, where T is the temperature, S is the volumic source, K is the material conductivity, C_p is the heat capacity and ρ is the material density. The boundary conditions for the thermal model are chosen to be a constant 20°C temperature at the bottom interface (set in the experiment by the temperature of the submount), and a zero thermal flux on every other boundaries.

Optics EXPRESS

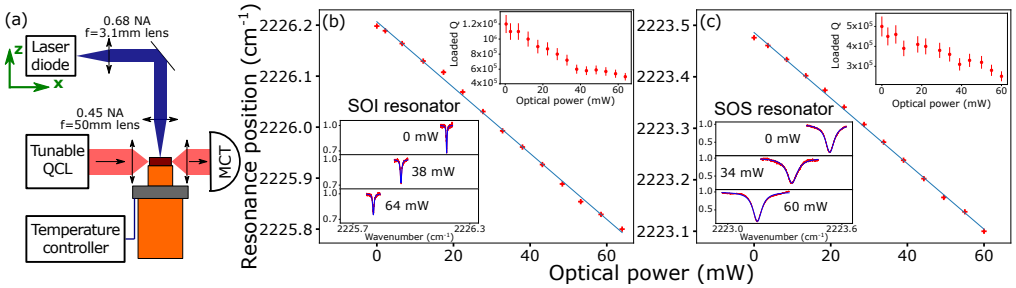

Fig. 2. (a) Schematic of the optical setup: a laser diode, a collimating lens and a focusing lens are added to the previous setup shown in Fig. 1(a). The laser position and the position of its focal point can be adjusted with a 3D-controlled stage. The position of the resonance is measured while changing the optical power of the heating laser for (b) the SOI resonator and (c) the SOS resonator. For both resonators, the resonance is tuned by about 0.4 cm^{-1} with 60 mW. Bottom-left inset: the transmitted QCL signal plotted as a function of the wavenumber at three different optical powers, shows the shift of the resonance. Top-right inset: the quality factor of the resonance with a 10% error bar is plotted as a function of the optical power of the heating laser.

$$-K\Delta T = \frac{S}{\rho C_p} \tag{1}$$

The absorption coefficient of silicon [17] and glass silica [18] at a wavelength of 450 nm are respectively $\alpha_{Si} = 26000\,cm^{-1}$, and $\alpha_{SiO_2} = 0.02\,cm^{-1}$. As light is absorbed in the silicon, hot electrons are created which thermalize by emiting phonons. The characteristic length of the electron thermalization in silicon [19], is shorter than the optical absorption length, meaning that the heat generation in silicon can be macroscopically modeled by the optical absorption. The optical power reflected at the air-silicon interface is calculated using the Fresnel coefficient, assuming a refractive index of 4.68 at 450 nm. The absorbed part of the light into the silicon is thus assumed to be 58% of the incident power.

We first consider a uni-dimensional stack similar to the SOI wafer used for making the SOI resonators (see. Fig. 3(a)). This stack is illuminated by a uniform light beam at a wavelength of 450 nm that can be modeled as a constant volume source in the first silicon layer. Under this approximation, the temperature profile can be solved analytically, and the solution of the stationary heat equation is a piece-wise linear function of the position z where the slope is proportional to the inverse of the thermal conductivity of the material K_{layer}. The temperature thus decreases much more in the SiO_2 layer and the thickness of this layer therefore has a great influence on the value of the temperature of the top layer. The temperature profile for an incident power of 64 mW on a circular surface of radius 100 µm is plotted on the right part of Fig. 3(a). This simple model shows how the thermal conductivity of SiO_2 influences significantly the temperature of the top layer. In particular, to enhance thermal effects in a ring resonator the thickness of SiO_2 should be as large as possible.

The resonator is now modeled in accordance with the three-dimensional schematic shown in Fig. 1(a). The solution of the stationary equation is computed with the thermal transfer module of Comsol Multiphysics with the respective volume heat source in the Si and SiO_2 layers S_{Si} and S_{SiO_2}.

We consider the case when the tuning laser beam is Gaussian with a spot is centered on the resonator. The heat source is thus modeled as a volume source with a Gaussian distribution in the radial direction, and an exponential decay in the z direction centered on the resonator as written in Eq. (2). P_0 and P_0' are the optical power absorbed by each material (P_0' then depends on the

Optics EXPRESS

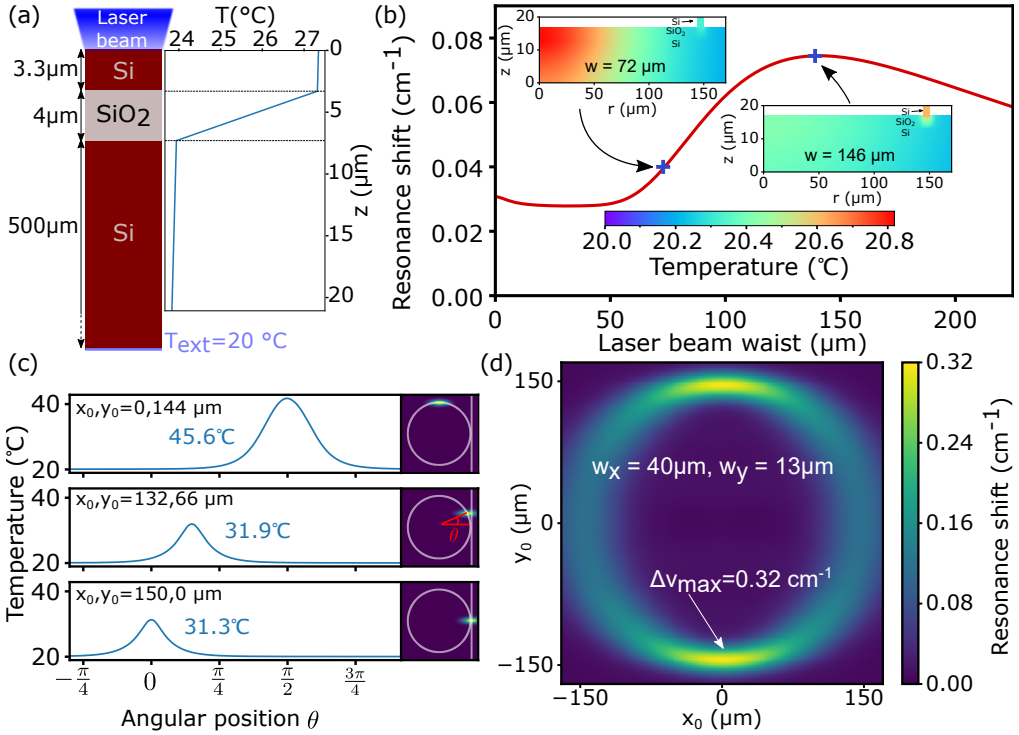

Fig. 3. (a) Uni-dimensional model of a SOI stack heated by light. The temperature profile is plotted as a function of the height z in the layer. (b) Three-dimensional thermo-optical model of the ring resonator showing the expected shift of the resonance for a beam centered on the resonator with a variable waist. Inset: temperature map of a cross-section of the resonator for two values of the waist. (c) For a beam with dimension $w_x = 40$ µm, $w_y = 13$ µm, the temperature profile along the resonator is plotted as a function of the angular coordinate for different beam positions. (d) Map showing the expected resonance shift as a function of the beam position on the sample.

geometry of the upper layer). The temperature in the ring resonator is studied as a function of the beam waist w.

$$S_{\mathrm{Si}} = \frac{\alpha_{\mathrm{Si}} P_0}{\pi w^2} e^{-\alpha_{\mathrm{Si}} z} e^{-\frac{r^2}{w^2}} \qquad S_{\mathrm{SiO_2}} = \frac{\alpha_{\mathrm{SiO_2}} P_0'}{\pi w^2} e^{-\alpha_{\mathrm{SiO_2}} z} e^{-\frac{r^2}{w^2}} \tag{2}$$

The resulting temperature maps are plotted for a radial cross-section of the ring for two different values of the beam waist in the inset of Fig. 3(b). These plots show that the temperature is nearly constant in the first silicon layer; therefore the effective temperature of the ring resonator is computed as the averaged temperature on its volume. From the average temperature of the resonator, we can compute the expected resonance shift by using the thermal dependence determined in the previous study using the TEC. The expected shift is then plotted in Fig. 3(b) as a function of the beam waist. The shift is found to be maximal when the beam waist is around 146 µm. Indeed, when the beam is centered in the middle of the ring resonator, the optimal heating is obtained when the spot is large enough to overlap with the ring while keeping the incident power inside of it. This study shows that focusing the beam at the center of the ring does not provide a large shift of the resonance on the SOI platform, because most of the energy is dissipated within the silicon substrate and therefore does not actively participate in heating the resonator. However, even when the beam is centered on the substrate, a non-zero shift of the

Optics EXPRESS

resonance remains. This thermo-optical tuning technique is thus suitable in situations where the resonator material does not absorb at the tuning laser wavelength.

We now consider a more general case where the tuning laser beam can be positioned anywhere on the resonator, and this spot is now modeled by an asymmetric Gaussian distribution corresponding to the experimental setup (waist: $w_x = 40\,\mu\text{m}$,$w_y = 13\,\mu\text{m}$) centered at coordinates x_0, y_0. The heat sources in both materials are now expressed in Eq. (3) and the stationary heat equation is solved with Comsol Multiphysics.

$$S_{\text{Si}} = \frac{\alpha_{\text{Si}} P_0}{\pi w_x w_y} e^{-\alpha_{\text{Si}} z} e^{-\left(\frac{(x-x_0)^2}{w_x^2} + \frac{(y-y_0)^2}{w_y^2}\right)} \qquad S_{\text{SiO}_2} = \frac{\alpha_{\text{SiO}_2} P_0'}{\pi w_x w_y} e^{-\alpha_{\text{SiO}_2} z} e^{-\left(\frac{(x-x_0)^2}{w_x^2} + \frac{(y-y_0)^2}{w_y^2}\right)} \tag{3}$$

The temperature along the resonator now depends on the angle θ, as plotted in Fig. 3(c) for beams centered in different positions. The actual beam spot is plotted on the side of each sub-plot. We observe the following regarding the position-dependence of the blue laser beam: the temperature in the resonator is higher when the spot is focused on the ring at positions such that the tangent to the ring is parallel to the x-axis. This condition results in a larger overlap between the spot and the ring, due to the ellipticity of the beam, and thus results in more heat dissipated within the resonator. For a perfectly circular spot one expect that the maximum temperature reached inside the resonator would not depend on the spot position along the ring angular coordinate.

Because of this temperature profile inside the resonator $T_r(\theta)$, the effective index $n(T)$ along the ring depends on the angular position: $n(T_r(\theta))$. The relative change of index with temperature is determined by using the result from the experiment with the TEC shown in section 2. The relative shift of the frequency of the p-th mode of the resonator ν_p can be expressed by Eq. (4).

$$\frac{\Delta\nu_p}{\nu_p} = \frac{\nu_p(T_0) - \nu_p(T)}{\nu_p(T_0)} = \frac{\frac{1}{2\pi R n(T_0)} - \frac{1}{\int_0^{2\pi} n(T_r(\theta)) R d\theta}}{\frac{1}{2\pi R n(T_0)}} = 1 - \frac{2\pi n(T_0)}{\int_0^{2\pi} n(T_r(\theta)) d\theta} \tag{4}$$

The shift in resonance is then mapped for different values of x_0 and y_0, for given values of w_x and w_y that correspond to the measured values of the laser beam, and for the SOI geometry. The corresponding map map is plotted in Fig. 3(d) for the beam waist obtained with our optical system (see Section 2). This figure shows that a tightly focused beam should enable a shift of the resonance of about $0.32\,\text{cm}^{-1}$, and that the maximum of the shift should be observed when the beam is focused on the ring itself. This absolute shift of the resonance is comparable to the shift observed experimentally in Fig. 3.

3.3. Mapping of SOS resonator

As with the SOI resonator, the SOS resonator is studied numerically. The stack is modeled as shown in the schematic in Fig. 1. In addition to the previously defined parameters, the sapphire is supposed to be transparent at 450 nm and we assume $\alpha_{\text{Al}_2\text{O}_3} = 0\,\text{cm}^{-1}$. There is only a single heat source for this model which is given in Eq. (5).

$$S_{\text{Si}} = \frac{\alpha_{\text{Si}} P_0}{\pi w_x w_y} e^{-\alpha_{\text{Si}} z} e^{-\left(\frac{(x-x_0)^2}{w_x^2} + \frac{(y-y_0)^2}{w_y^2}\right)} \tag{5}$$

The numerical study of the expected resonance shift is done similarly as in the previous section. In Figs. 4(a) and 4(b) the expected shift is respectively plotted for a tightly focused spot ($w_x = 40\,\mu\text{m}$, $w_y = 13\,\mu\text{m}$) and less a focused spot ($w_x = 49\,\mu\text{m}$, $w_y = 106\,\mu\text{m}$). The results show an expected shift of at most $0.46\,\text{cm}^{-1}$ and $0.36\,\text{cm}^{-1}$ respectively.

The dependence of the resonance shift on the spatial position of the spot is then studied experimentally to check the consistency of the model. The surface of the SOS resonator is

Optics EXPRESS

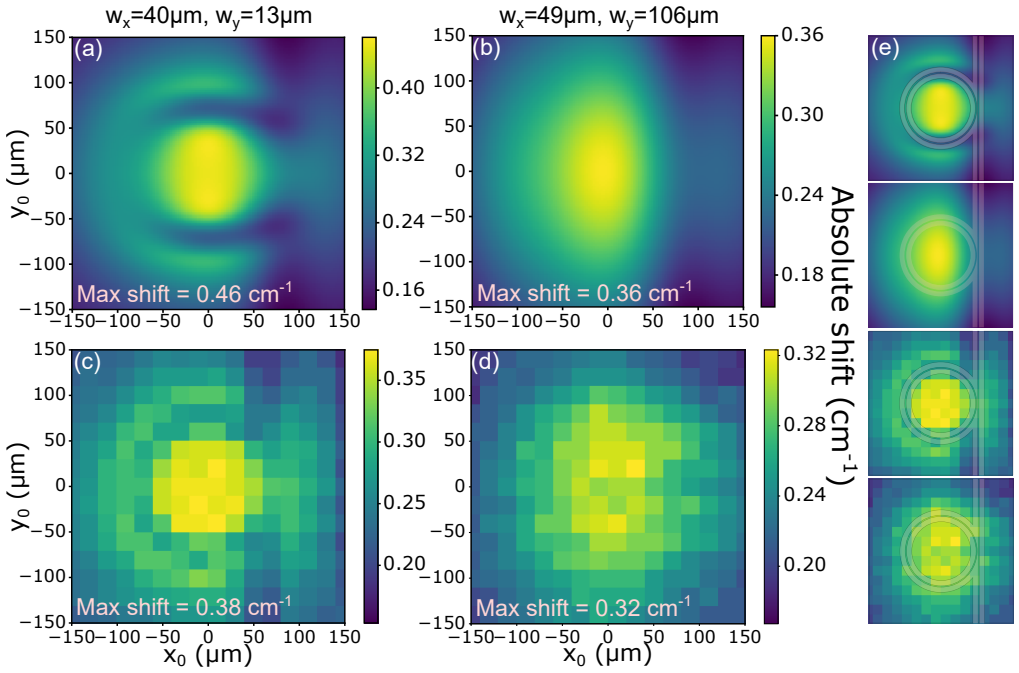

Fig. 4. The simulated resonance shift for the SOS resonator is plotted as function of the position of the spot on the resonator sample for different sizes of spot w_x, w_y: (a) $w_x = 40\,\mu m$, $w_y = 13\,\mu m$ and (b) $w_x = 49\,\mu m$, $w_y = 106\,\mu m$. The resonance shift is measured as a function of the position and plotted for two configurations corresponding to the measured spot sizes: (c) $w_x = 40\,\mu m$, $w_y = 13\,\mu m$ and (d) $w_x = 49\,\mu m$, $w_y = 106\,\mu m$. (e) The four previous maps are shown superposed with the silicon ring and waveguide.

scanned with the tuning laser spot on a region of size 300 µm by 300 µm centered on the resonator. This mapping is done for both a focused and defocused laser beam previously characterized and the results are shown in Figs. 4(c) and 4(d). Experimentally, the shift of the resonance under the laser illumination was found to be at most $0.38\,cm^{-1}$ for the smaller spot size and $0.32\,cm^{-1}$ for the larger spot. With these maps, we distinguish the geometric features of the resonator device, as enhanced in Fig. 4(e) by showing an overlay of resonator and waveguide on the previously described maps. Overall the experimental measurement and the numerical simulations show a similar dependence of the resonance shift as a function of the spot position. Especially, the maximum shift is obtained when the spot is positioned at the center of the ring. This result highlights the locality of the direct thermo-optical tuning method.

However, the actual magnitude of the resonance shift differs between both results. This can be explained since our model is purely thermal and does not consider the dispersion due to a change of free-carrier concentration. One can estimate the increase in carrier concentration [20] based on the variation of the quality factor through the absorption coefficient. This increase in carrier density was evaluated at $3.5 \times 10^{15}\,cm^{-3}$ for the highest illumination power in the SOI resonator (assuming equal concentrations of holes and electrons). This increased carrier concentration creates a free-carrier dispersion, that results in an optical index decrease of 1.7×10^{-4}. Such a decrease in refractive index would then result in a increase of the resonance frequency by about $0.1\,cm^{-1}$, thus opposing the thermal shift. Figure 4 shows a difference between experiment and simulation of the same order of magnitude. The modeled evolution of the maps while changing the spot size corresponds to the theory, and show that a reasonable shift of the resonance does not require precise focusing and can be achieved with a large spot size.

Optics EXPRESS

4. Study of the frequency response of the laser tuning

During the previous measurements, the response of the resonator to the heating laser was observed to be faster than when tuning the temperature with TEC. In order to characterize this behavior more quantitatively, a frequency response measurement of the system was performed.

The previous setup is modified as follows: a different EC-QCL is used (Daylight Solutions HHG-41045) and its emission is tuned to a fixed single-mode frequency. The heating laser current is now modulated by a sinusoidal wave of variable frequency by using a custom made power supply, such that that the output power responds linearly in the range of the modulation. By this process, the illumination of the resonator and thus its resonance frequency are periodically modulated by this signal. The experiment starts with an initially blue-detuned pump laser positioned near the transmission minimum at resonance. As the heating laser intensity rises, the resonance frequency decreases and the pump moves out of the resonance (see blue curve in Fig. 5(a)). As the laser intensity decreases, the resonator cools and its resonance frequency increases and eventually goes back to the initial state.

For this experiment, the laser current was obtained by measuring the voltage across a 5 Ω resistor in series with the laser diode while detecting the mid-IR light transmitted through the resonator chip. We measured the response of the laser light modulation as a function of the laser current for different frequencies by using a 1 ns rise-time photodiode under reverse bias (Thorlabs DET10A, bandwidth 350 MHz). Thanks to the measurement of this transfer function, we are able to plot the detected mid-IR signal as a function of the actual laser power for different frequencies.

Figures 5(c) and 5(d) show the recorded mid-IR signals and the laser power over one period for different modulating frequencies for the SOI and SOS resonators. The left panel shows as a function of time the normalized laser power (black dashed curve) and the transmitted mid-IR signal normalized by the peak-to-peak amplitude at lower frequencies. The right panel shows orbits of the mid-IR signal with the same normalization as a function of the absolute laser power.

The latter orbits are particularly meaningful to study the phase difference between the tuning signal and the transmitted signal. At low frequencies, the intensity of the detected light follows the heating signal well. A linear growing curve means that the signals are in phase and an ellipse shows a significant phase shift between the two signals. Around 10 kHz for the SOI (resp. 1 kHz for the SOS), the shape of the orbits changes to an ellipse as the transmitted mid-IR light gets out of phase with the laser modulation. This effects gets stronger for higher frequencies, until it gets dephased by almost π compared to the tuning signal.

In Figs. 5(e) and 5(f) the normalized resonator response, defined as the integral of the product of the laser current and the detected mid-IR signal, is plotted as a function of the frequency. Physically this represents the correlation between the heating laser power and the transmitted light through the resonator sample. The cut-off frequency can be extracted from this curve by extrapolation of the decreasing slope. We thus estimated the cut-off frequency of this technique to be around 10 kHz for the SOI and around 1 kHz for the SOS resonator. In inset of these two figures, the phase difference between the laser power and the transmitted light is plotted. As observed on the ellipses the phase difference increases from the cut-off frequency to a final value at 1 MHz slightly under π as the frequency increases. We also plotted the modulation depth, defined as the peak-to-peak amplitude of the modulated mid-IR signal normalized by the peak-to-peak amplitude of the laser power. The modulation depth slowly decreases and then strongly increase after the cut-off frequency for the SOI resonator, while it decreases for the SOS resonators.

We explain the two extreme values for the phase difference as follows: first at low frequencies, the heating of the resonator follows the modulation of the laser diode, which results in a near-zero phase difference. In the high frequency limit (while remaining of the order a 1 MHz) heating effects stop playing a role. At the same time, free-carriers are still being generated by

Optics EXPRESS

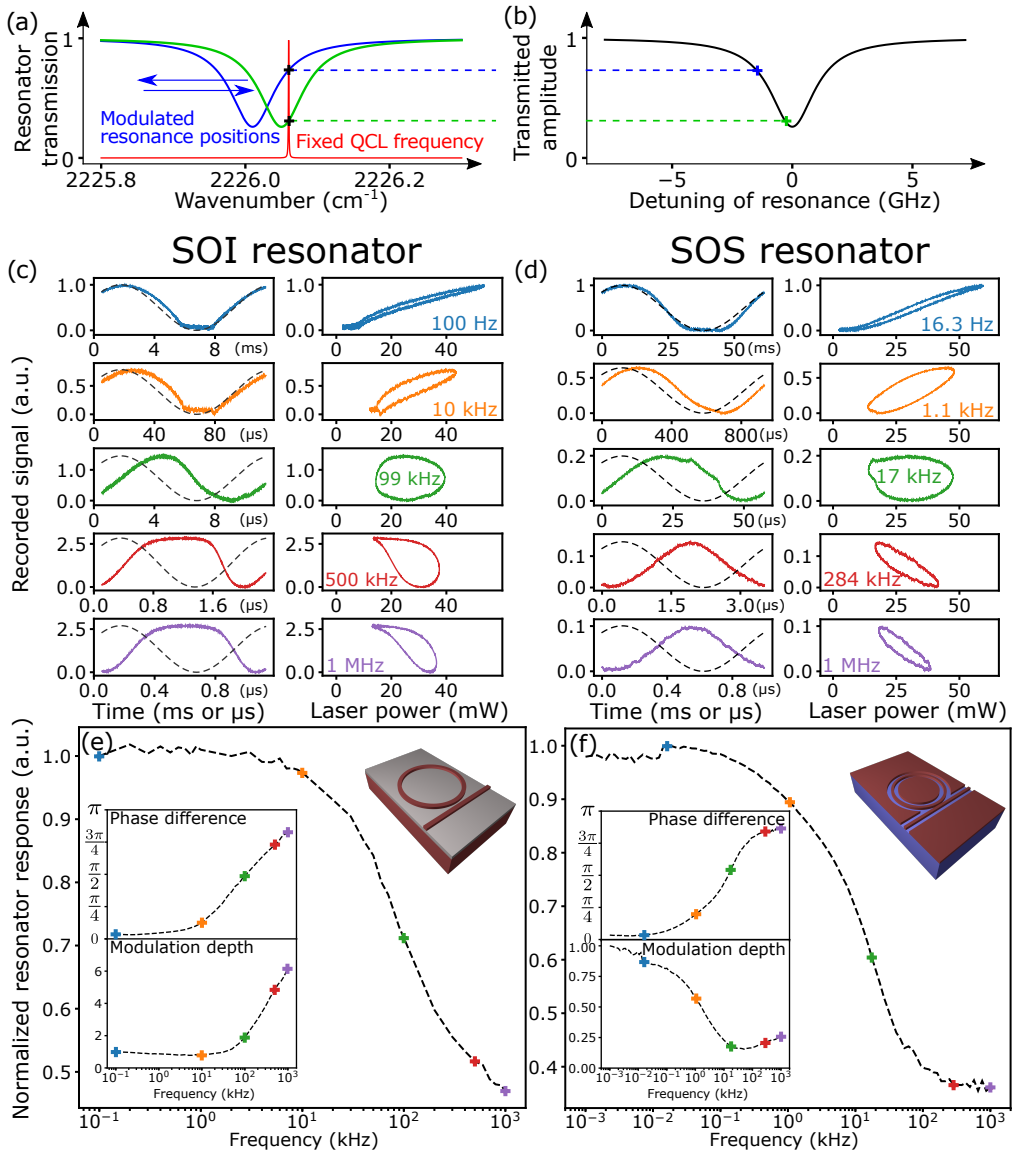

Fig. 5. (a-b) The ring resonance is modulated and the QCL frequency is fixed. The transmitted signal varies accordingly with the detuning of the resonator. The relative value of both the normalized laser power and transmitted optical power signals are plotted, first over time, and then one as a function of the other in (c) for the SOI resonator, and in (d) for the SOS resonator. The color of the curves correspond to the dots shown in (e-f). The normalized response of the resonator, defined as the product of the normalized laser power and of the out-coupled signal from the resonator, is plotted as function of the modulation frequency for: (e) the SOI resonator, (f) the SOS resonator. In inset of (e) and (f) we plotted the phase difference between the laser power and the detected mid-IR signal and the modulation depth of the mid-IR signal. This modulation depth corresponds to the peak-to-peak amplitude of the mid-IR signal normalized by the peak-to-peak amplitude of the laser power.

Optics EXPRESS

the absorption of blue light in silicon, as this is a fast process. The increase in free-carriers concentration has one significant effect: it decreases the optical index in the ring resonator due to free carrier dispersion. This effect is opposed to that of thermal tuning as it shifts the resonance towards higher frequencies under strong illumination, and towards lower frequencies under weak illumination. Therefore the effect of the modulation of the free carriers concentration on the transmitted mid-IR signal has the opposite sign compared to the laser intensity modulation. As a consequence, in the high frequency limit, a π phase difference between the laser power and the mid-IR signal is expected. In between the two limit behaviors, the phase difference can take any value between 0 and π.

The domination of free-carriers effect at higher frequency also explains the different behavior of the modulation depth for the two resonators. According to the simulations, and since we optimized the position of the laser spot on the resonator during this experiment, we can assume that the laser spot was on the ring of the SOI resonator and near the center of the SOS ring. This configuration would result in more free-carriers generation in the SOI resonator, while limiting this effect in the SOS resonator. As a consequence, one may expect a smaller change in amplitude due to the free-carrier generation in the SOS resonator compared to the SOI resonator.

5. Conclusions

We demonstrated experimentally for SOI and SOS resonators that a blue laser diode can be used to directly their resonance by about $0.4\,\mathrm{cm}^{-1}$. This method was found to be local, non-invasive, linear and capable of modulation frequencies up to 10 kHz. The experimental results are supported by numerical modeling of the temperature within a resonator.

While the magnitude of the resonance tuning observed was limited compared to the figure obtained with a pure thermal tuning by using a TEC, the thermo-optical tuning can still be used as a fine tuning method. Practically for microresonator comb generation, one would tune the resonator as close a possible to the pump laser using the TEC, and then use the thermo-optical tuning for the final and high precision tuning. The measurement of the Q-factor of the resonance under blue light illumination shows that while free carriers are created their effect can be mitigated by keeping the laser power under a predefined threshold. Combining this method with a TEC cooler for coarse tuning would ensure that the laser power is kept low and that the resonator losses are not affected by the tuning method. Thanks to the fast response measured here, this method is also suitable to be used in a closed control loop scheme [10], ensuring the stability of the optical signal exiting the resonator. This technique for tuning a ring resonator is particularly useful for the mid-IR where some tunable sources suffer from mode-hopping and cannot be continuously tuned into a ring resonance. As opposed to the integration of micro-heaters onto a resonator sample this method does not involve depositing metal and the increase in ring losses caused by the tuning laser illumination is reversible, thus we can qualify this method as non-invasive.

This work, motivated here by the tuning of microresonators for frequency comb generation can be extended to other on-chip silicon photonic devices that can benefit from thermal tuning [10] such as filters, interferometers or multiple-ring structures [21]. Thanks to the local nature of this tuning method and its fast response, one may envision to extend this scheme to independent and time-dependant tuning sources focused on different components of a chip, achieving new optical functions in the mid-infrared. This method can also be extended to other integrated platforms for microresonators such as silicon nitride by choosing the emission wavelength of the heating laser to match either the absorption of the resonator material or of its substrate.

Funding

DARPA SCOUT (W31P4Q-16-1-0002); National Science Foundation (NSF) (ECCS-1614631,1541959).

Optics EXPRESS

Acknowledgments

This work was supported by the DARPA SCOUT program through Grant No. W31P4Q-16-1-0002. We acknowledge support from the National Science Foundation under Award No. ECCS-1614631. This work was performed in part at the Center for Nanoscale Systems (CNS), a member of the National Nanotechnology Coordinated Infrastructure Network (NNCI) which is supported by the National Science Foundation under NSF Award no. 1541959. Any opinions, findings, conclusions or recommendations expressed in this material are those of the authors and do not necessarily reflect the views of the Assistant Secretary of Defense for Research and Engineering or of the National Science Foundation.

References

1. T. J. Kippenberg, R. Holzwarth, and S. A. Diddams, "Microresonator-based optical frequency combs," Science **332**, 555–559 (2011).
2. Y. Okawachi, K. Saha, J. S. Levy, Y. H. Wen, M. Lipson, and A. L. Gaeta, "Octave-spanning frequency comb generation in a silicon nitride chip," Opt. Lett. **36**, 3398–3400 (2011).
3. M. Yu, Y. Okawachi, A. G. Griffith, M. Lipson, and A. L. Gaeta, "Mode-locked mid-infrared frequency combs in a silicon microresonator," Optica **3**, 854–860 (2016).
4. A. Hugi, G. Villares, S. Blaser, H. C. Liu, and J. Faist, "Mid-infrared frequency comb based on a quantum cascade laser," Nature **492**, 229–233 (2012).
5. D. Kazakov, M. Piccardo, Y. Wang, P. Chevalier, T. S. Mansuripur, F. Xie, C.-e. Zah, K. Lascola, A. Belyanin, and F. Capasso, "Self-starting harmonic frequency comb generation in a quantum cascade laser," Nat. Photonics **11**, 789–792 (2017).
6. P. Chevalier, M. Piccardo, S. Anand, E. A. Mejia, Y. Wang, T. S. Mansuripur, F. Xie, K. Lascola, A. Belyanin, and F. Capasso, "Watt-level widely tunable single-mode emission by injection-locking of a multimode fabry-perot quantum cascade laser," Appl. Phys. Lett. **112**, 061109 (2018).
7. A. Spott, E. J. Stanton, N. Volet, J. D. Peters, J. R. Meyer, and J. E. Bowers, "Heterogeneous integration for mid-infrared silicon photonics," IEEE J. Sel. Top. Quantum Electron. **23**, 1–10 (2017).
8. T. Herr, K. Hartinger, J. Riemensberger, C. Wang, E. Gavartin, R. Holzwarth, M. L. Gorodetsky, and T. Kippenberg, "Universal formation dynamics and noise of kerr-frequency combs in microresonators," Nat. Photonics **6**, 480–487 (2012).
9. S. B. Papp, P. Del'Haye, and S. A. Diddams, "Mechanical control of a microrod-resonator optical frequency comb," Phys. Rev. X **3**, 031003 (2013).
10. K. Padmaraju and K. Bergman, "Resolving the thermal challenges for silicon microring resonator devices," Nanophotonics **3**, 269–281 (2014).
11. X. Xue, Y. Xuan, C. Wang, P.-H. Wang, Y. Liu, B. Niu, D. E. Leaird, M. Qi, and A. M. Weiner, "Thermal tuning of Kerr frequency combs in silicon nitride microring resonators," Opt. Express **24**, 687–698 (2016).
12. C. Joshi, J. K. Jang, K. Luke, X. Ji, S. A. Miller, A. Klenner, Y. Okawachi, M. Lipson, and A. L. Gaeta, "Thermally controlled comb generation and soliton modelocking in microresonators," Opt. Lett. **41**, 2565–2568 (2016).
13. V. R. Almeida, C. A. Barrios, R. R. Panepucci, and M. Lipson, "All-optical control of light on a silicon chip," Nature **431**, 1081–1084 (2004).
14. R. Shankar, I. Bulu, and M. Lončar, "Integrated high-quality factor silicon-on-sapphire ring resonators for the mid-infrared," Appl. Phys. Lett. **102**, 051108 (2013).
15. S. A. Miller, M. Yu, X. Ji, A. G. Griffith, J. Cardenas, A. L. Gaeta, and M. Lipson, "Low-loss silicon platform for broadband mid-infrared photonics," Optica **4**, 707–712 (2017).
16. T. Carmon, L. Yang, and K. J. Vahala, "Dynamical thermal behavior and thermal self-stability of microcavities," Opt. Express **12**, 4742–4750 (2004).
17. C. Schinke, P. Christian Peest, J. Schmidt, R. Brendel, K. Bothe, M. R. Vogt, I. Kröger, S. Winter, A. Schirmacher, S. Lim *et al.*, "Uncertainty analysis for the coefficient of band-to-band absorption of crystalline silicon," AIP Adv. **5**, 067168 (2015).
18. S. T. Yang, M. J. Matthews, S. Elhadj, D. Cooke, G. M. Guss, V. G. Draggoo, and P. J. Wegner, "Comparing the use of mid-infrared versus far-infrared lasers for mitigating damage growth on fused silica," Appl. Opt. **49**, 2606–2616 (2010).
19. J. Yang, E. Ziade, and A. J. Schmidt, "Modeling optical absorption for thermoreflectance measurements," J. Appl. Phys. **119**, 095107 (2016).
20. M. Nedeljkovic, R. Soref, and G. Z. Mashanovich, "Free-carrier electrorefraction and electroabsorption modulation predictions for silicon over the 1–14-μm infrared wavelength range," IEEE Photon. J. **3**, 1171–1180 (2011).
21. B. G. Lee, B. A. Small, Q. Xu, M. Lipson, and K. Bergman, "Characterization of a 4×4 gb/s parallel electronic bus to wdm optical link silicon photonic translator," IEEE Photon. Technol. Lett **19**, 456–458 (2007).